ELSEVIER

Biophysical Chemistry 108 (2004) 187–200

Biophysical Chemistry

www.elsevier.com/locate/bpc

A model for sedimentation in inhomogeneous media. I. Dynamic density gradients from sedimenting co-solutes

Peter Schuck*

Division of Bioengineering and Physical Science, ORS, OD, National Institutes of Health, Building 13, Room 3N17, 13 South Drive, Bethesda, MD 20892-5766, USA

Abstract

Macromolecular sedimentation in inhomogeneous media is of great practical importance. Dynamic density gradients have a long tradition in analytical ultracentrifugation, and are frequently used in preparative ultracentrifugation. In this paper, a new theoretical model for sedimentation in inhomogeneous media is presented, based on finite element solutions of the Lamm equation with spatial and temporal variation of the local solvent density and viscosity. It is applied to macromolecular sedimentation in the presence of a dynamic density gradient formed by the sedimentation of a co-solute at high concentration. It is implemented in the software SEDFIT for the analysis of experimental macromolecular concentration distributions. The model agrees well with the measured sedimentation profiles of a protein in a dynamic cesium chloride gradient, and may provide a measure for the effects of hydration or preferential solvation parameters. General features of protein sedimentation in dynamic density gradients are described.

Keywords: Sedimentation velocity; Analytical ultracentrifugation; Finite element methods; Density gradient centrifugation; Isopycnic separation; Size distributions; Lamm equation

1. Introduction

The sedimentation of macromolecules through inhomogeneous media is a process frequently encountered in the practice of centrifugation. Density gradient techniques in preparative ultracentrifuges have a great importance as general biochemical tools. In analytical ultracentrifugation, density gradient sedimentation has a long history for the study of nucleic acids [1–3], the molar mass and buoyant density of proteins [4], and it is still applied in a variety of studies with topics ranging from the composition of genomes [5–7] to the characterization of protein–detergent and protein–lipid complexes [8,9]. Smaller self-forming density gradients generated by the centrifugal field are the basis of analytical zone centrifugation [10,11], and gradients in solvent density and viscosity may also be generated inadvertently at high centrifugal fields when using high concentrations of a sedimenting co-solute, such as sucrose. In the field of synthetic polymer chemistry, isopycnic density gradient ultracentrifugation is an important assay for the characterization of macromolecules and particles, for example in industrial processes [12].

The theoretical prediction and the analysis of macromolecular transport in density gradients is

*Tel.: +1-301-435-1950; fax: +1-301-480-1242.
E-mail address: pschuck@helix.nih.gov (P. Schuck).

0301-4622/04/$ - see front matter © 2003 Published by Elsevier B.V.
doi:10.1016/j.bpc.2003.10.016

significantly more complex than the standard sedimentation in homogeneous solvents for thermodynamic and computational reasons. A variety of models were proposed in earlier studies. Several authors addressed the migration of a sedimenting band in a hypothetical pre-existing density and/or viscosity gradient [13–16]. As part of their pioneering theoretical work on the characterization and analysis of macromolecular sedimentation profiles in the ultracentrifuge, Yphantis and co-workers have first considered the evolution of the solvent density distribution with time [17]. They used an empirical formula for the relaxation kinetics of the distribution of a co-solute acting as densifier, and solved the macromolecular redistribution in the dynamic gradient with the flow equation for macromolecular sedimentation and diffusion in the centrifugal field, the Lamm equation [18]. In this work, the simplifying assumption of a rectangular geometry was made [17]. Sartory et al. have used a finite-difference solution of the Lamm equation to describe the sedimentation of the small co-solute, and developed approximate analytical expressions for the sedimentation and diffusion of a thin band of macromolecules in the dynamic density gradient, using an equilibrium perturbation technique [19]. Minton has developed a finite-difference method for predicting the non-ideal sedimentation of CsCl, and described a finite-difference algorithm to approximate the sedimentation of a macromolecular species in the density gradient [20].

In the last decade, the analysis of transport processes in analytical ultracentrifugation underwent significant development. The application of improved mathematical and computational tools now permits the efficient and precise solution of the Lamm equation, which can be used to characterize macromolecular sedimentation coefficients, molar masses, size-distributions and molecular interactions [21–32]. However, this development was constrained to sedimentation in homogeneous solvents.

In the present paper, a general model is proposed for macromolecular sedimentation in inhomogeneous media. It is based on finite-element solutions of the Lamm equation with a dynamic description of the local density and viscosity, derived from the non-ideal sedimentation of a co-solute. It can also be applied to the sedimentation in compressible solvents, which is described in the second paper of this series [33]. The model is implemented in the software SEDFIT and can be used for the prediction of macromolecular sedimentation, as well as for the analysis of experimentally measured macromolecular concentration profiles from the analytical ultracentrifuge. The model is tested with experimental data from the sedimentation of a protein in CsCl solution, and several features of macromolecular sedimentation in inhomogeneous media are described.

2. Theory

2.1. Finite element solution of the Lamm equation in inhomogeneous solvents

The Lamm equation describes the sedimentation and diffusion of a macrosolute in the sector-shaped volume of the analytical ultracentrifuge:

$$\frac{\partial c}{\partial t} = \frac{1}{r}\frac{\partial}{\partial r}\left[rD\frac{\partial c}{\partial r} - s\omega^2 r^2 c\right] \qquad (1)$$

with $c(r, t)$ denoting the concentration at a distance r from the center of rotation and at time t, ω the angular velocity, D the diffusion coefficient and s the sedimentation coefficient. Although it is strictly not valid for three-component systems [34], it may be used as a first approximation for macromolecular sedimentation for cases where interactions between the macrosolute and co-solute can be neglected or approximated as a constant change in the apparent partial-specific volume of the macrosolute. In this approximation, gradients in density and viscosity due to the redistribution of co-solute will be treated as a background on which macromolecular sedimentation and diffusion according to Eq. (1) takes place. Limitations of this approximation will be discussed below.

If we consider the effect of locally varying solvent viscosity η and density ρ on the macromolecular sedimentation, it is useful to relate the local macromolecular transport parameters to those under standard conditions:

$$D_{\exp}(r,\ t)=\frac{\eta_{20,w}}{\eta(r,\ t)}D_{20,w}=:\alpha(r,\ t)D_{20,w} \tag{2a}$$

$$s_{\exp}(r,\ t)=\frac{\eta_{20,w}}{\eta(r,\ t)}\left(\frac{1-\phi'\rho(r,\ t)}{1-\bar{v}\rho_{20,w}}\right)s_{20,w} =:\alpha(r,\ t)\beta(r,\ t)s_{20,w} \tag{2b}$$

with the partial-specific volume of the macromolecule $\bar{v}$, with the standard conditions denoted with the index 20,w (for water at 20 °C), with the apparent partial-specific volume ϕ' (which includes hydration and preferential solvation), and with the abbreviation α denoting the inverse of the relative viscosity, and with β denoting the relative buoyancy. It should be noted that if the density of the macromolecule $1/\bar{v}$ is close to the solvent density, changes in the relative buoyancy can be very large even at small changes in solvent density. The thermodynamically correct form of the buoyancy factor is the density increment $(d\rho/dc)_\mu$ [35]. It is expressed here in an equivalent form with an apparent partial-specific volume $(1-\phi'\rho(r,\ t))$, from which preferential interaction coefficients of water and co-solute may be calculated [36] (Section 4).

Although the Lamm equation (Eq. (1)) does not have an analytical solution, it can be solved very efficiently by finite element techniques [24,25,37]. Following the method outlined in Ref. [24], we can approximate the concentration distribution $c(r,\ t)$ as a superposition of elements P_k

$$c(r,\ t)\approx\sum_{k=1}^{N}c_k(t)P_k(r,\ t) \tag{3}$$

which are based on a grid of N radial points that divide the sample from meniscus m to bottom b:

$$P_1(r,\ t)=\begin{cases}(r_2-r)/(r_2-r_1) & \text{for } r_1\le r\le r_2\\ 0 & \text{else}\end{cases} \tag{4a}$$

$$P_N(r,\ t)=\begin{cases}(r-r_{N-1})/(r_N-r_{N-1}) & \text{for } r_{N-1}<r\leqslant r_N\\ 0 & \text{else}\end{cases} \tag{4b}$$

and for $k=2,\ldots,N$:

$$P_k(r,\ t)=\begin{cases}(r-r_{k-1})/(r_k-r_{k-1}) & \text{for } r_{k-1}<r\leqslant r_k\\ (r_{k+1}-r)/(r_{k+1}-r_k) & \text{for } r_k<r\leqslant r_{k+1}\\ 0 & \text{else}\end{cases} \tag{4c}$$

As introduced first by Claverie [37], the elements P_k can be constant and equidistant triangular hat functions ($r_{k+1}=r_k+\Delta r$). A more efficient and numerically more stable choice of elements, in particular for small D, is a moving frame of reference, in which the radial grid points r are logarithmically spaced and time-dependent [24]. If the $r_k(t)$ evolve exponentially according to $r_k(r)=r_{k,0}\exp(s_G\omega^2(t-t_0))$ (with s_G denoting a sedimentation coefficient), they mimic the sedimentation of non-diffusing particles and can provide a frame of reference that is translated and stretched so that the sedimentation term in Eq. (1) disappears and Eq. (1) reduces to the description of diffusion alone. Details on efficient spatial and temporal discretization schemes can be found in Ref. [24]. The following discussion will proceed in a general way with non-equidistant and time-dependent elements P_k, in which the equations for a Claverie grid are contained as a special case with $\partial P_k/\partial t=0$.

Analogous to the macromolecular concentration, we can also use the elements P_k to express the local viscosity term α and the relative buoyancy β as

$$\alpha(r,\ t)=\sum_{k=1}^{N}\alpha_k(t)P_k(r,\ t)$$
$$\beta(r,\ t)=\sum_{k=1}^{N}\beta_k(t)P_k(r,\ t) \tag{5}$$

Multiplication of both sides of Eq. (1) with an element P_k and volume integration from meniscus to bottom (using integration by parts and taking advantage of the vanishing total flux at meniscus and bottom) leads to

$$\int_m^b \frac{\partial c}{\partial t} P_k r \mathrm{d}r = s_{20,\mathrm{w}}\omega^2 \int_m^b \alpha\beta c \frac{\partial P_k}{\partial r} r^2 \mathrm{d}r - D_{20,\mathrm{w}} \int_m^b \alpha \frac{\partial c}{\partial r}\frac{\partial P_k}{\partial r} r \mathrm{d}r \quad (6)$$

Inserting Eqs. (3) and (5) leads to the set of linear equations

$$\sum_j \frac{\mathrm{d}c_j}{\mathrm{d}t}\int_m^b P_j P_k r \mathrm{d}r + \sum_j c_j \int_m^b \frac{\partial P_j}{\partial t} P_k r \mathrm{d}r = s_{20,\mathrm{w}}\omega^2 \sum_j c_j \sum_{l,n} a_l \beta_n \int_m^b P_l P_n P_j \frac{\partial P_k}{\partial r} r^2 \mathrm{d}r - D_{20,\mathrm{w}} \sum_j c_j \sum_l a_l \int_m^b P_l \frac{\partial P_j}{\partial r}\frac{\partial P_k}{\partial r} r \mathrm{d}r \quad (7)$$

which can be written in matrix form

$$\sum_j \left(\frac{\mathrm{d}c_j}{\mathrm{d}t}\mathbf{B}_{kj} + c_j s_{\mathrm{G}} \mathbf{A}^{(3)}_{kj} \right) = \sum_j c_j \left(s_{20,\mathrm{w}}\omega^2 \sum_{l,n} a_l \beta_n \mathbf{A}^{(2^*)}_{ln,kj} - D_{20,\mathrm{w}} \sum_l a_l \mathbf{A}^{(1^*)}_{l,kj} \right) \quad (8)$$

In Eq. (8), the matrices $\mathbf{B}_{kj}$ and $s_{\mathrm{G}}\mathbf{A}^{(3)}_{kj}$ are as described in Ref. [24], and analytical expressions for the new matrices $\mathbf{A}^{(1^*)}(t) = \sum_l \alpha_l \mathbf{A}^{(1^*)}_{l,kj}$ and $\mathbf{A}^{(2^*)}(t) = \sum_{l,n} \alpha_l \beta_n \mathbf{A}^{(2^*)}_{ln,kj}$ are given in Appendix A. In comparison with the case of homogeneous solvent, the matrices $\mathbf{A}^{(1^*)}(t)$ and $\mathbf{A}^{(2^*)}(t)$ appear in place of the usual propagation matrices $\mathbf{A}^{(1)}$ and $\mathbf{A}^{(2)}$ [24]. In fact, it can be shown that the sum over the tensor elements equals those previous propagation matrices, i.e. $\sum_l \mathbf{A}^{(1^*)}_{l,kj} = \mathbf{A}^{(1)}_{kj}$ and $\sum_{l,n} \mathbf{A}^{(2^*)}_{ln,kj} = \mathbf{A}^{(2)}_{kj}$. This can be expected because the constant homogeneous solvent conditions should emerge as a special case from Eq. (8) when constant buoyancy and relative viscosity coefficients are used. Eq. (8) can be solved with methods similar to those described earlier for the case of a moving frame of Ref. [24] and for the Claverie scheme [25]. For time-dependent density and viscosity gradients, the propagation matrices have to be updated after each time-increment. The finite element solution was incorporated in the software SEDFIT, which can be downloaded from www.analyticalultracentrifugation.com.

2.2. Dynamic density gradients formed by sedimenting co-solutes

Gradients in density and viscosity can be established during the centrifugation experiment by sedimentation of a co-solute in high concentration. The mutual diffusion coefficient of such a component is given by

$$D = \frac{kT\upsilon}{f}\left(1 + w\frac{\mathrm{d}\ln\gamma}{\mathrm{d}w}\right) \quad (9)$$

where k is the Boltzmann constant, T is the absolute temperature, υ is the dissociation number, f the frictional coefficient, γ the thermodynamic activity coefficient and w the weight concentration of the co-solute [38]. Following the approximation that the frictional coefficient for sedimentation and diffusion is approximately identical for the solutes under consideration, such as CsCl, the sedimentation coefficient can be written as

$$s = \frac{M(1-\bar{\upsilon}\rho_0)D}{\upsilon RT(1 + w\mathrm{d}\ln\gamma/\mathrm{d}w)} \quad (10)$$

(with M denoting the molar mass of the species and ρ_0 the solvent density) [20]. Minton has given polynomial approximations for the sedimentation and mutual diffusion coefficient of CsCl solutions, and applied them to the simulation of self-forming CsCl density gradients using a finite difference solution of the Lamm equation [20]. A similar approach is implemented in SEDFIT, using the polynomial approximations for the concentration dependence of $D(c)$ and $s(c)$ combined with a finite element solution of the Lamm equation [25,39]. For the simulation of sedimentation of a dilute macromolecular component in the self-form-

ing density gradient, the evolution of the co-solute is coupled to the solution of the Lamm equation for the macromolecular components, and from the local concentration of the co-solute, the local density and viscosity experienced by the macromolecular component are calculated.

As an alternative approach, SEDFIT allows one to empirically model experimental data from the redistribution of a co-solute, assign a molar loading concentration of this species, and use its redistribution as a basis for calculating $\rho(r, t)$ and $\eta(r, t)$. This approach is simpler, as it does not require the measurement of the full concentration dependence $D(c)$ and $s(c)$. Apparent D and s-values at the loading concentration may be modeled, for example, to interference optical data of the co-solute alone with water as an optical reference, run separately in the same rotor. Although this approach may appear less rigorous, it is sufficient to calculate the local density and viscosity effects if the co-solute redistribution can be described well.

3. Results

Because the Lamm equation is notoriously difficult to solve and no analytical solution exists, it is crucial to verify the precision and the limitations of the algorithm. The present method was tested according to several different criteria. First, the sedimentation of a 200-kDa protein in a linear density and viscosity gradient was simulated, sufficient to generate a band with neutral buoyancy at approximately 7.1 cm. Both the static and the moving frame of reference algorithms independently converged to the same solution. While static frame of reference algorithm converged rapidly with finer spatial grid (maximal relative error $\delta_{max} < 10^{-5}$ at grid size $n > 500$), the moving frame of reference required a significantly finer spatial grid to converge to the same solution ($\delta_{max} < 3 \times 10^{-4}$ at $n = 20\,000$, $\delta_{max} = 5 \times 10^{-3}$ at $n = 1000$). This indicates that the moving frame of reference does not lend itself to sedimentation under conditions that include regions of neutral buoyancy. However, this effect was significantly reduced in shallower density gradients that do not lead to band formation. Under these conditions, the moving frame of reference was advantageous when solving the Lamm equation for large macromolecules that sediment rapidly. As a second test of the algorithm, it was verified that mass conservation is fulfilled, and that it solved the Lamm equation correctly for the special cases of constant viscosity and density, which is identical to the sedimentation in homogeneous solvents after correction of s and D to standard conditions. Third, the sedimentation of a macromolecule in a large linear density gradient was simulated, and it was verified that the calculated distribution after long times converged to the thermodynamically predicted equilibrium distribution of a Gaussian band with the correct molar mass and density (Eq. 5.260 of Ref. [40]). Finally, the Lamm equation solution was found to be consistent with an approximate analytical solution for the special case of diffusion-free sedimentation in a density gradient from compressible solvents [33].

The model for inhomogeneous media was incorporated in several sedimentation models of SEDFIT for the prediction and modeling of macromolecular sedimentation through a dynamically formed density and viscosity gradient. Two different experimental configurations were explored. Fig. 1 (top panel) shows the changes in density across the solution column from the sedimentation of 2.5 M CsCl after conventional uniform loading. As the co-solute concentration increases close to the bottom, conditions for neutral buoyancy and flotation for a protein are generated (top panel, bold line). The calculated sedimentation profiles of a hypothetical 500-kDa protein is shown in the middle and lower panel. The initial sedimentation resembles the ordinary formation of a boundary in the meniscus region and the accumulation of material with a steep gradient close to the bottom of the cell. After a short time, however, the increasing density of the co-solute at the bottom causes the macromolecule to float back from the bottom of the cell towards the evolving point of neutral buoyancy. Combined with the continuing sedimentation from the sedimentation boundary in the meniscus region, this process concentrates the protein in a peak that approaches the Gaussian shape well known for isopycnic sedimentation (Fig. 1, middle panel). Clearly, the calculated

macromolecular sedimentation profiles contain information about its molar mass, sedimentation coefficient, as well as partial-specific volume.

Even if the co-solute concentration is far below the threshold required to establish neutral buoyancy of the macromolecule, its redistribution can cause significant effects on the macromolecular concentration profiles. This is illustrated in Fig. 2, which shows the concentration distribution of a 200-kDa protein sedimenting in 1 M CsCl. While the macromolecular sedimentation takes place, the co-solute also redistributes and spans concentrations from 0.76 M near the meniscus to 1.29 M near the bottom (at the end of the time interval shown in Fig. 2). This leads to a deceleration of the sedimentation boundary as compared to the sedimentation in a uniform solvent (dotted line in Fig. 2). More striking is a concentration increase in the 'plateau' region towards the bottom of the cell. This is not due to back-diffusion, but due to the differentially decreasing sedimentation rate with higher radii, a consequence of which is the continuous accumulation of material in the region that forms the plateau in homogeneous solvents. A similar effect has been observed by Dishon et al. in the approximate Lamm equation solutions in the rectangular geometry [17]. However, a qualitatively new feature is a negative slope in the 'plateau' region close to the boundary. This is a result of the dilution of the co-solute, which locally increases the buoyant molar mass and sedimentation coefficient of the macromolecules. This increase can produce sedimentation coefficients higher than those at the hinge point of the co-

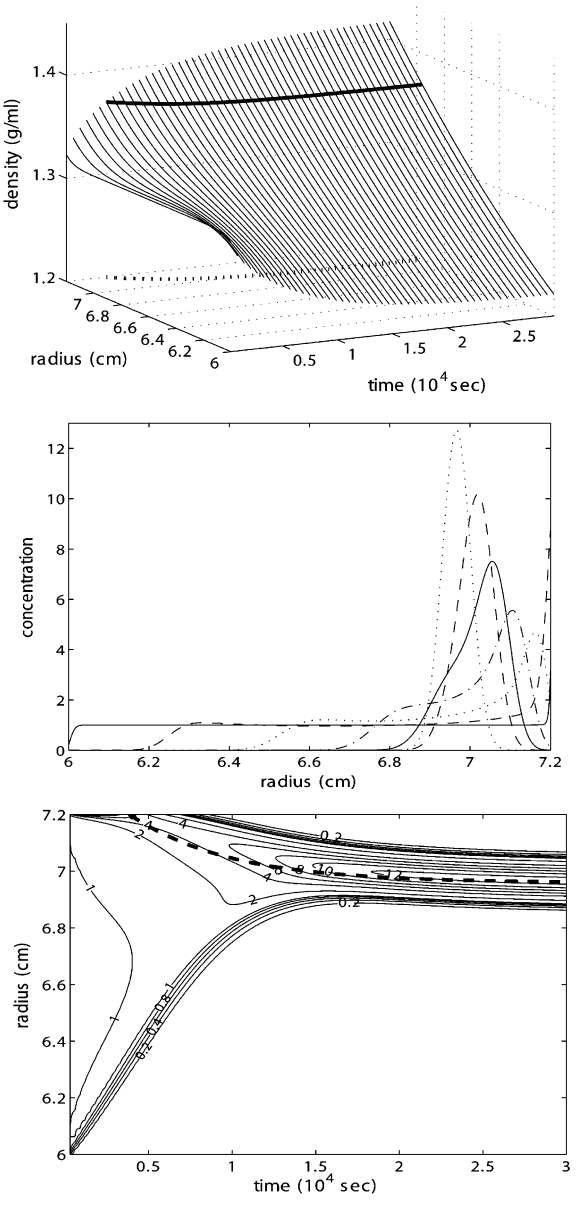

Fig. 1.

Fig. 1. Sedimentation in a self-forming density gradient in conventional loading configuration. Top panel: calculated density profiles generated by the sedimentation of 2.5 M CsCl at 60 000 rpm (in time-intervals of 600 s). The initial density is 1.31 g/ml, which is below the density of neutral buoyancy for a protein of partial-specific volume 0.73 ml/g. With time, the increase in concentration close to the bottom generates densities that permit flotation of the protein. The evolution of the point of critical density (1.37 g/ml) is shown as a bold solid line, and its projection to the radius–time plane as a dotted line. Middle panel: sedimentation profiles of a protein with a molar mass of 500 kDa, a partial-specific volume of 0.73 ml/g, and a sedimentation coefficient of $s_{20,w} = 18$ S. Shown are the concentration distributions at 300 s (solid line), 3000 s (dashed line), 6000 s (dotted line), 9000 s (dash-dotted line), 12 000 s (solid line), 15 000 s (dashed line) and 30 000 s (dotted line). Lower panel: contour plot of the evolution of the macromolecular concentration distribution. (It should be noted that the time-scale is in 10^4 s, which does not permit resolving the very early stages that are included in the middle panel.) The bold dotted line indicates the radii with neutral buoyancy conditions calculated from the sedimentation of the co-solute, as shown in the Top panel.

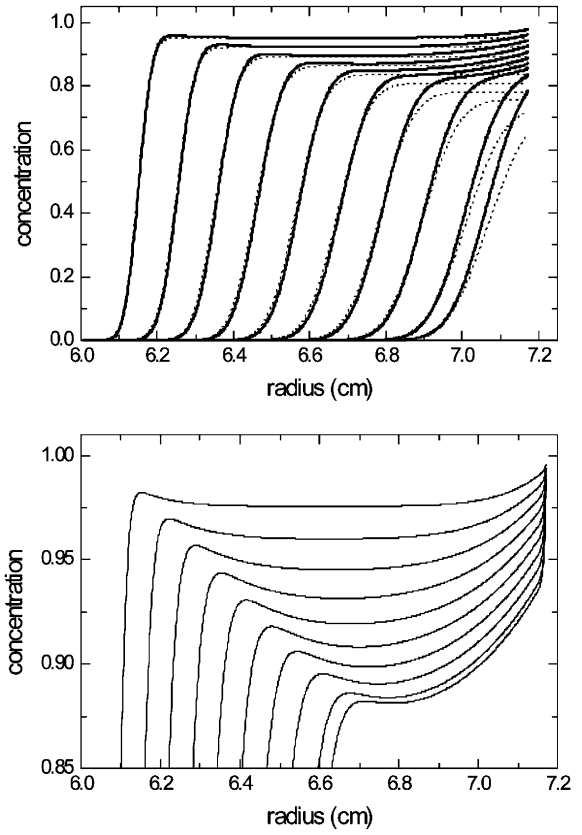

Fig. 2. Sedimentation in a self-forming density gradient in conventional loading configuration with lower concentration of co-solute. Top panel: concentration distributions calculated for a 200-kDa protein ($\bar{v}=0.73$ ml/g, $s_{20,w}=10$ S) sedimenting at 60 000 rpm in 1 M CsCl. Data are shown with time-intervals of 600 s. For comparison, the sedimentation profiles calculated for a constant homogeneous solvent at $\rho=1.126$ g/ml and $\eta=0.952$ mPa s (the density and viscosity of 1 M CsCl) are shown as dotted lines. Lower panel: detailed view of the plateau region of the calculated concentration profiles for a protein of 150 kDa with a sedimentation coefficient $s_{20,w}$ of 5 S sedimenting at 60 000 rpm in 1 M CsCl.

solute, and thus lead to an accumulation of material at the leading edge of the boundary. This effect was found to be more pronounced with a lower ratio of the macromolecular to the co-solute sedimentation coefficient (Fig. 2, lower panel).

The model was implemented in SEDFIT for the non-linear regression of macromolecular sedimentation parameters, given sets of experimental concentration distributions. When normally distributed noise (1% of the loading signal) was added to the data in Figs. 1 and 2, they could be analyzed with the independent species model similar to ordinary sedimentation velocity data in homogeneous solvents, but with the effective partial-specific volume as an additional (optional) fitting parameter (data not shown). All parameters converged to the values underlying the simulations, although slightly slower than in the case of uniform solvents. Slower convergence is attributed to some correlation between the effective partial-specific volume and the remaining parameters, in particular at the smaller density gradients.

As an experimental test for the validity of the presented model for the sedimentation in dynamic density gradients, sedimentation velocity experiments in cesium chloride solutions were performed. Fig. 3 shows the absorbance profiles of a 83-kDa protein in 1.43 M cesium chloride (initial density 1.183 g/ml). The sedimentation profiles are substantially different from those obtained in dilute solution (data not shown). Qualitatively, the data confirm the predicted deceleration of the boundary and the compression of the scans in the bottom region, as well as the increasing slope of the 'plateau' near the bottom region in the later scans (Fig. 3). It should be noted that at the conditions used this region is free of back-diffusion (as measured by control experiments at lower CsCl concentration). Also visible is the predicted boundary anomaly from the local density decrease in the half of the solution column closer to the meniscus, which leads to a transient small negative slope of the 'plateau' (Fig. 3, lower panel). This effect is here less pronounced than calculated in the simulation of Fig. 2 due to the larger diffusion coefficient of the protein. However, it has been reproducibly observed in further experiments at high CsCl concentration (data not shown).

For the quantitative analysis, the polynomial expressions of Ref. [20] for $D(c)$ and $s(c)$ were used to predict the sedimentation of CsCl, and the resulting density and viscosity profiles were inserted in the Lamm equation model. Because of the high rotor speed, corrections for the compressibility of water were also included (although this effect is smaller than that of the redistribution of the co-solute) [33,48]. The non-linear regression

showed some correlation between the apparent partial-specific volume, the sedimentation coefficient, and the bottom position of the centrifuge cell. Therefore, the $s_{20,w}$ value was held constant at 5.05 S, the value predicted from hydrodynamic modeling of the crystal structure [41], which compares well with the value of 5.01 S measured in phosphate buffered saline (PBS), and the bottom location was estimated from a initial scan of the transmitted intensity. Also fixed were the molar mass and the partial-specific volume of the protein under standard conditions, both calculated from the amino acid sequence. With the meniscus position and the apparent partial-specific volume ϕ' of the protein in 1.43 M cesium chloride as the only floating parameters, a reasonable fit with a root-mean-square (rms) deviation of 0.0099 OD was achieved (Fig. 3, solid lines), with $\phi' = 0.762$ ml/g. (When time-invariant noise was considered in the model, the fit converged to a value of $\phi' = 0.760$ ml/g, with an rms deviation of 0.0064 OD, data not shown.) The increase in the apparent partial-specific volume in the presence of 1.43 M cesium chloride would correspond to a hydration of 0.20 g/g, if there was no preferential binding of the co-solute to the protein, although the latter cannot be excluded. Overall, a reasonable quantitative and a very good qualitative agreement of the experimental data with the Lamm equation model was found, supporting the validity of the model.

A second configuration theoretically explored was a self-forming density gradient in the synthetic boundary configuration of analytical zone centrifugation [10]. Fig. 4 shows the simulated co-solute and macromolecular distributions for a dilute solution of protein which is layered on top of a solution containing 2.5 M CsCl. Although a relatively small density difference (e.g. from 150 mM NaCl) is

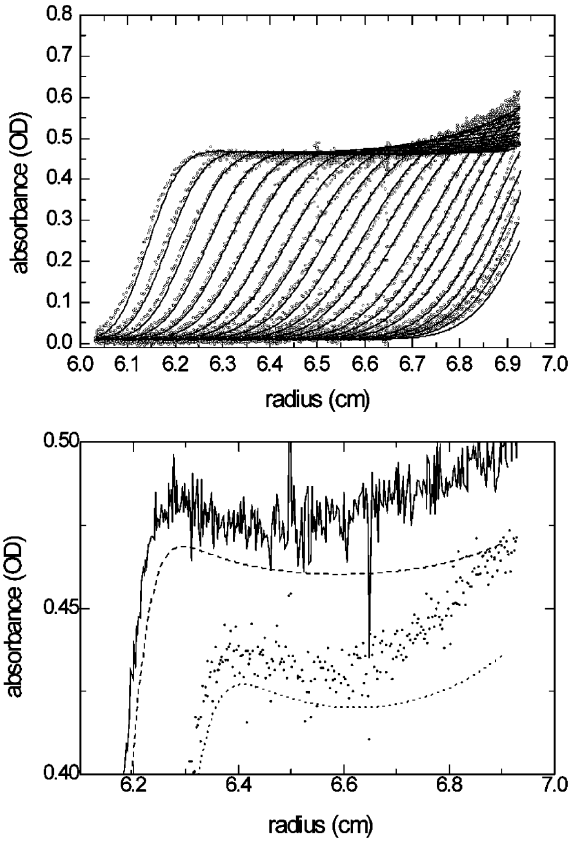

Fig. 3.

Fig. 3. Experimental absorbance profiles from the sedimentation of a protein in a dynamic density gradient (circles) and best-fit model (solid lines). Anthrax protective antigen [50] was diluted at a concentration of 0.45 mg/ml into PBS with 1.43 M CsCl (initial density 1.183 g/ml), and sedimented at a rotor speed of 60 000 rpm and a rotor temperature of 25 °C in an Optima XLA/I analytical ultracentrifuge (Beckman Coulter, Fullerton, CA). Data shown in the upper panel are the absorbance profiles measured at 280 nm in time intervals of 730 s. The data were modeled using finite element Lamm equation solutions for the sedimentation of CsCl (with the polynomial approximations for the non-ideal sedimentation parameters reported in Ref. [20]), together with tabulated data for the concentration dependences of the density and viscosity of CsCl solutions [51] for dynamically updating the local density and viscosity in the Lamm equation solution Eq. (8) for the sedimentation of the protein. Also included were corrections for the compressibility of water [33]. For fitting the data, the known protein molar mass and the partial specific volume $\bar{\upsilon}$ from the amino acid sequence was used, and its sedimentation coefficient $s_{20,w}$ was fixed to the value of 5.05 S predicted from the crystal structure [41]. The apparent partial specific volume ϕ' was treated as fitting parameter (together with the meniscus of the solution column), converging to a value of 0.762 ml/g with a final rms deviation of the fit of 0.0099 OD. The lower panel provides a more detailed view of the boundary anomaly due to the hydrostatic interaction of the protein and the co-solute: the experimental scans at 2570 s (solid line) and 4030 s (circles) are shown and the corresponding theoretical profiles (for clarity, the scans are offset).

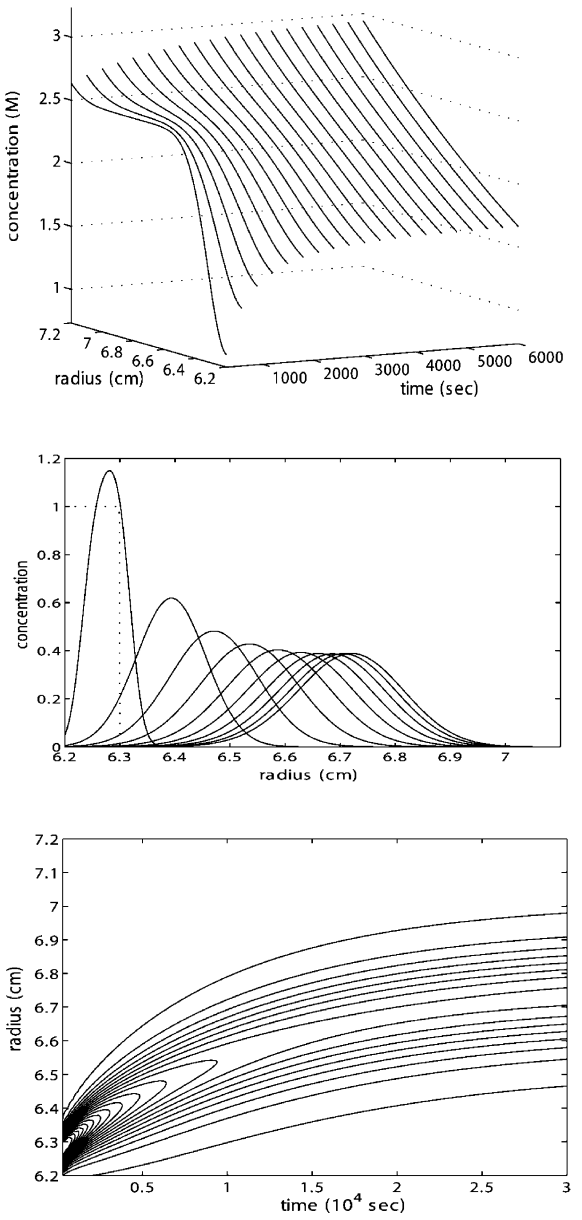

Fig. 4. Simulated analytical zone centrifugation in a self-forming density gradient. The distributions are calculated for a 1-mm layer of a protein solution in PBS on top of a 9 mm solution of PBS with 2.5 M CsCl, at 60 000 rpm and 25 °C. For the protein, a molar mass of 82.7 kDa, a $s_{20,w}$—value of 5 S, and $\bar{\upsilon}=0.77$ ml/g was assumed, with a loading concentration of 1. Top panel: calculated redistribution of CsCl with time. Middle panel: protein distributions at time intervals of 3000 s (first distribution shown at 300 s). The dotted line indicates the protein layer at the start of centrifugation. Lower panel: contour plot of the evolution of the protein concentration distribution.

sufficient for gravitational stability of the protein layer, the purpose of the high CsCl concentration in the present context is to generate a density gradient that permits isopycnic separation of species with different density [13]. The top panel in Fig. 4 shows the redistribution of the CsCl, its diffusion into the protein lamella with a steep concentration gradient, and the formation of a concentration gradient along the whole solution column. In this configuration, the CsCl gradient is established more rapidly than in the homogeneous loading conditions (Fig. 1). The protein distributions are indicated in the middle and lower panel of Fig. 4. Interestingly, due to the steep initial density gradient an initial concentration of the protein in the region of the lamella takes place, analogous to the boundary anomaly in the conventional loading situation. Under some conditions, this effect was predicted to produce a series of initial band profiles increasing in height, qualitatively consistent with experimental scans (J. Lebowitz, unpublished observation). After this period of concentration, the band broadens again and approaches the position of neutral buoyancy. In the simulations, it was found that the extent of this sharpening effect strongly depends on the initial density gradient, and the macromolecular diffusion and sedimentation coefficient. Small diffusion coefficients were also found to generate stronger asymmetry of the bands. As in the conventional loading configuration, the implementation in SEDFIT permits analytical zone centrifugation data to be modeled to extract molar mass, effective partial-specific volume, and the sedimentation coefficient $s_{20,w}$ from experimental data.

4. Discussion

The sedimentation of macromolecules through inhomogeneous solvents is of great practical importance, but its theoretical description is highly complex. In the present paper, a new theoretical model is presented for the sedimentation in dynamic gradients from sedimenting co-solutes. For the first time, the model permits the prediction of the complete evolution of the macromolecular concentration profiles across the solution column, and

can be used to analyze experimentally measured macromolecular concentration distributions, similar to whole boundary modeling approaches in homogeneous solvents. Although the model is based on several simplifying assumptions, it still captures essential features and provides a realistic picture of the sedimentation process, as judged by the agreement with the experimental data from the sedimentation of a protein in high CsCl solutions.

One limitation of the model is that it is based on the two-component Lamm equation, which is strictly valid only if cross-terms in the diffusion coefficients are negligible (Eq. 1.61–1.63 in Ref. [34]). In theory, this requirement is fulfilled in the absence of interaction of the macromolecule with the co-solute, and negligible preferential solvation. Clearly, many conditions where density gradients are used in practice will violate this requirement, and this may constitute a serious drawback for a detailed quantitative analysis of the measured boundary shapes. However, the analysis of experimental data (Fig. 3) indicates that even in the presence of significant preferential solvation, its consequences can apparently be captured well by a change in the macromolecular density increment, or apparent partial-specific volume, without considering flows from cross-diffusion. This indicates that under the conditions used, contributions to the macromolecular flows from cross-diffusion may be small, possibly due to the fact that the relative concentration gradients of the co-solute remain small, even though they can already generate a significant mechanical effect on the macromolecular buoyancy. Further, the model also neglects the dependence of the solvation on the local co-solute concentration, and treats it instead as being constant throughout the entire sedimentation process. Again, this approximation may be justified if the relative changes of co-solute concentration remain small throughout the solution column. These simplifications seemed to still provide a realistic picture of the sedimentation process in Fig. 3, but more experience will be required to generalize this observation, and to explore if the observed change in buoyancy allows to quantitatively measure hydration or preferential solvation parameters [36]. (It should be noted that these considerations about co-solute sedimentation and redistribution are only of second order or negligible, if the effects of co-solutes are evaluated from a series of experiments with different loading concentrations of co-solute or macromolecules. Also, it should be noted that many co-solutes may not generate significant density gradients.)

Frequently, the characterization of proteins is desired in the presence of high concentrations of co-solutes, where preferential solvation occurs. For example, co-solutes may be required for stabilizing proteins, or for density matching of detergents in the study of membrane proteins. Preferential solvation can also be very important in the context of protein–protein interactions induced by protein–solvent interactions [42,43]. The current method could extend sedimentation velocity as a quantitative tool to conditions where such co-solutes generate density gradients. It should be noted that the whole boundary modeling method is exquisitely sensitive and that the effect of density gradients may be measured at co-solute concentrations where preferential solvation is absent or small, such as with dynamic density gradients produced by H_2O/D_2O mixtures.

Most of the qualitative features in the macromolecular sedimentation profiles caused by density gradients are well known. Beyond flotation and the formation of an isopycnic band, which usually requires relatively high densities, there are also profound changes in the sedimentation profiles at much lower densities. These consist in a deceleration of the sedimentation boundary, which results in the continuous accumulation of macromolecules in the region where in homogeneous solvents a constant plateau would be formed [17]. This is also observed in static density gradients from compressible solvents [44,45]. A boundary anomaly that is characteristic for the dynamic nature of the density gradient is the local inversion of the leading edge of the boundary (lower panels in Figs. 2 and 3). The inversion is gravitationally stabilized by the underlying density gradient of the co-solute. This feature may appear not unlike the Johnston–Ogston effect [46,47], although the interaction is mediated through hydrostatic density effects between a sedimenting small co-solute and a macromolecule, rather than the hydrodynamic interaction between two macromolecules. In ana-

lytical zone centrifugation, the anomaly corresponding to the boundary inversion is an initial sharpening of the bands to concentrations above the loading concentration.

It is clear that the analysis procedures for uniform solvents cannot be applied to density gradient sedimentation. Even at co-solute concentrations that do not lead to flotation, the boundary distortions do not permit modeling without consideration of the gradient. For example, because of the absence of a true plateau, no weight-average sedimentation coefficients can be defined through second-moment mass balance consideration [44]. As a first step to enable a more quantitative interpretation of density gradient centrifugation by direct boundary modeling, the Lamm equation model was implemented for non-linear regression with the independent species model of SEDFIT. This requires the prediction of the density gradient, which may be accomplished by taking sedimentation parameters from tabulated data in the literature, as in the present work, or by independently measuring the co-solute sedimentation profiles with the interference optical detection system. As can be expected, if sufficiently large gradients exist, this permits the determination of molar mass, sedimentation coefficient, and an effective partial-specific volume. Although the extension of the independent species analysis to a continuous sedimentation coefficient distribution $c(s)$ and molar mass distribution $c(M)$ [30] is possible, this approach was not explored. Since the sedimentation profile in density gradients can depend much stronger on the molar mass and partial-specific volume of the macromolecules than in homogeneous solvents, the approximation of a single weight-average frictional ratio for the entire macromolecular population may not be sufficient to model polydisperse mixtures. At conditions of strong density gradients and macromolecules that are heterogeneous with regard to their density, extensions to multi-dimensional distributions $c(s, \bar{v})$ or $c(s, M, \bar{v})$ may be required. One could expect that sedimentation data from the complete transport process towards an isopycnic separation condition contain enough information to define such an extended characterization of a macromolecular mixture.

Appendix A:

In the theory section, it was shown that the finite element solutions for sedimentation with buoyancy and viscosity gradients require the calculation of tensors

$$A^{(1*)}_{l,kj} = \int_m^b P_l\left(\partial P_j/\partial r\right)\left(\partial P_k/\partial r\right) r \mathrm{d}r$$

and

$$A^{(2*)}_{ln,kj} = \int_m^b P_l P_n P_j\left(\partial P_k/\partial r\right) r^2 \mathrm{d}r.$$

The functions P are defined as triangular hat functions according to Eqs. (4a), (4b) and (4c), based on a division of the solution column between the meniscus m and the bottom b into N radial grid points r_k (which can be static and equidistant, as in the Claverie scheme [37], or logarithmically spaced and time-dependent, as in the moving frame of Ref. [24]). Because they are overlapping only for identical or neighboring elements, the integral $\mathbf{A}^{(1*)}_{l,kj}$ is nonzero only if both l and j equal k, $k-1$ or $k+1$. Similarly, $\mathbf{A}^{(2*)}_{\mathrm{ln,kj}}$ is nonzero only if n, l and j equal k, $k-1$ or $k+1$. This considerably simplifies the calculations. The viscosity gradients $\alpha(r,t)$ and the buoyancy gradients $\beta(r,t)$ are expressed through the vectors $\alpha_l(t)$ and $\beta_n(t)$, respectively, which are defined via Eq. (5) on the same grid of radial points. This allows analytical expressions to be derived for the matrices

$$\mathbf{A}^{(1*)}(t) = \sum\nolimits_l \alpha_l \mathbf{A}^{(1*)}_{l,kj}$$

and

$$\mathbf{A}^{(2*)}(t) = \sum\nolimits_{l,n} \alpha_l \beta_n \mathbf{A}^{(2*)}_{ln,kj}$$

For the corner elements of $\mathbf{A}^{(1*)}(t)$ we obtain

$$\mathbf{A}^{(1*)}_{11} = \frac{r_1(2\alpha_1+\alpha_2)+r_2(\alpha_1+2\alpha_2)}{6(r_2-r_1)}$$
$$\mathbf{A}^{(1*)}_{NN} = \frac{r_N(2\alpha_N+\alpha_{N-1})+r_{N-1}(\alpha_N+2\alpha_{N-1})}{6(r_N-r_{N-1})} \quad \text{(A1a)}$$

and for all other elements

$$\mathbf{A}^{(1^*)}_{k,k-1}=\frac{r_k(2\alpha_k+\alpha_{k-1})+r_{k-1}(\alpha_k+2\alpha_{k-1})}{6(r_{k-1}-r_k)}$$
$$\mathbf{A}^{(1^*)}_{k,k+1}=\frac{r_k(2\alpha_k+\alpha_{k+1})+r_{k+1}(\alpha_k+2\alpha_{k+1})}{6(r_k-r_{k+1})}$$
$$\mathbf{A}^{(1^*)}_{k,k}=-\mathbf{A}^{(1)}_{k,k-1}-\mathbf{A}^{(1)}_{k,k+1} \qquad \text{(A1b)}$$

For the corner elements of $\mathbf{A}^{(2^*)}(t)$, we obtain

$$\mathbf{A}^{(2^*)}_{1,1}=-\frac{\beta_1\alpha_1}{60}(10r_1^2+4r_2r_1+r_2^2)$$
$$-\frac{\beta_2\alpha_1+\beta_1\alpha_2}{60}(2r_1^2+2r_2r_1+r_2^2)$$
$$-\frac{\beta_2\alpha_2}{60}(r_1^2+2r_2r_1+2r_2^2)$$
$$\mathbf{A}^{(2^*)}_{2,1}=-\mathbf{A}^{(2^*)}_{1,1}$$

$$\mathbf{A}^{(2^*)}_{N,N}=\frac{\beta_{N-1}\alpha_{N-1}}{60}\times(r_N^2+2r_Nr_{N-1}+2r_{N-1}^2)+\frac{\beta_N\alpha_N}{60}(r_N^2+4r_Nr_{N-1}+10r_N^2)+\frac{\beta_N\alpha_{N-1}+\beta_{N-1}\alpha_N}{60}\times(2r_N^2+2r_Nr_{N-1}+r_{N-1}^2)$$
$$\mathbf{A}^{(2^*)}_{N-1,N}=-\mathbf{A}^{(2^*)}_{N,N} \qquad \text{(A2a)}$$

and for all other elements

$$\mathbf{A}^{(2^*)}_{k,k-1}=\frac{\beta_{k-1}\alpha_{k-1}}{60}(r_k^2+2r_kr_{k-1}+2r_{k-1}^2)+\frac{\beta_k\alpha_{k-1}+\beta_{k-1}\alpha_k}{60}(2r_k^2+2r_kr_{k-1}+r_{k-1}^2)+\frac{\beta_k\alpha_k}{60}(10r_k^2+4r_kr_{k-1}+r_{k-1}^2)$$
$$-\frac{\beta_k\alpha_k}{60}(10r_k^2+4r_kr_{k+1}+r_{k+1}^2)-\frac{\beta_k\alpha_{k-1}+\beta_{k-1}\alpha_k}{60}(2r_k^2+2r_kr_{k+1}+2r_{k+1}^2)-\frac{\beta_{k+1}\alpha_{k+1}}{60}(r_k^2+2r_kr_{k+1}+2r_{k+1}^2)$$

$$\mathbf{A}^{(2^*)}_{k,k}=\frac{\beta_{k-1}\alpha_{k-1}}{60}(r_k^2+2r_kr_{k-1}+2r_{k-1}^2)+\frac{\beta_k\alpha_{k-1}+\beta_{k-1}\alpha_k}{60}\times(2r_k^2+2r_kr_{k-1}+r_{k-1}^2)+\frac{\beta_k\alpha_k}{60}\times(10r_k^2+4r_kr_{k-1}+r_{k-1}^2)-\frac{\beta_k\alpha_k}{60}\times(10r_k^2+4r_kr_{k+1}+r_{k+1}^2)-\frac{\beta_k\alpha_{k-1}+\beta_{k-1}\alpha_k}{60}\times(2r_k^2+2r_kr_{k+1}+r_{k+1}^2)-\frac{\beta_{k+1}\alpha_{k+1}}{60}\times(r_k^2+2r_kr_{k+1}+2r_{k+1}^2) \qquad \text{(A2b)}$$

If buoyancy and viscosity gradients are absent and all α_l and β_n equal unity, these elements $\mathbf{A}^{(1^*)}(t)$ and $\mathbf{A}^{(2^*)}(t)$ are identical to the matrices $\mathbf{A}^{(1)}$ and $\mathbf{A}^{(2)}$ for homogeneous solvent as given in Eqs. A2 and A3 in Refs. [24,49].

Interestingly, the tensor

$$\mathbf{A}^{(1^*)}_{l,kj}=\int_m^b P_l\left(\partial P_j/\partial r\right)\left(\partial P_k/\partial r\right)r\mathrm{d}r$$

underlying the matrix $\mathbf{A}^{(1^*)}(t)$ is identical to the tensor $\mathbf{W}_{kj,l}$ that was previously used to describe diffusion fluxes of macromolecules with hydrodynamic or thermodynamic non-idealities (Eq. A6 in Ref. [24]); essentially it describes any radially dependent diffusion. No relationship of the tensor $\mathbf{A}^{(2^*)}_{ln,kj}$ with any tensor previously used in the context of sedimentation is known. As an alternative to the approach presented here, it should be possible to also express the sedimentation fluxes in the presence of density and viscosity gradients within the framework previously derived for concentration dependent sedimentation (i.e. using the tensors $\mathbf{U}_{kji}$ defined in Eq. A5 in Ref. [24]), if one reduces the product of the local viscosity and buoyancy into a single radial-dependent factor. However, as can be seen from the cross-terms of neighboring buoyancy and viscosity coefficients in Eq. (A2b) above, this approach would exhibit lower accuracy. Further, use of the previously

described framework with tensors **U** and **W** is numerically less efficient, in particular for static solvent gradients. It is more advantageous, therefore, to employ the expressions for the matrices $\mathbf{A}^{(1*)}$ and $\mathbf{A}^{(2*)}$ given above to replace the ordinary propagation matrices $\mathbf{A}^{(1)}$ and $\mathbf{A}^{(2)}$ as described in the theory section.

These matrix elements, their relationships, and the corresponding expressions in C code were derived using the symbolic mathematics toolbox of MATLAB (The Mathworks, Natick, MA), and can be obtained from the author on request.

References

[1] M. Meselson, F.W. Stahl, The replication of DNA in *Escherichia coli*, Proc. Natl. Acad. Sci. USA 44 (1958) 671.

[2] C. Schildkraut, J. Marmur, P. Doty, Determination of the base composition of deoxyribonucleic acid from its buoyant density in CsCl, J. Mol. Biol. 4 (1962) 430–443.

[3] J. Vinograd, J. Lebowitz, R. Radloff, R. Watson, P. Laipis, The twisted circular form of polyoma viral DNA, Proc. Natl. Acad. Sci. 53 (1965) 1104–1111.

[4] J.B. Ifft, Sedimentation equilibrium of proteins in density gradients, Biophys. Chem. 5 (1976) 137–157.

[5] O. Clay, N. Carels, C. Douady, G. Macaya, G. Bernardi, Compositional heterogeneity within and among isochores in mammalian genomes. I. CsCl and sequence analyses, Gene 276 (2001) 15–24.

[6] O. Clay, Standard deviations and correlations of GC levels in DNA sequences, Gene 276 (2001) 33–38.

[7] G. Bucciarelli, G. Bernardi, An ultracentrifugation analysis of two hundred fish genomes, Gene 295 (2002) 153–162.

[8] A. Lustig, A. Engel, M. Zulauf, Density determination by analytical ultracentrifugation in a rapid dynamic gradient—application to lipid and detergent aggregates containing proteins, Biochem. Biophys. Acta 1115 (1991) 89–95.

[9] Z. Bozoky, L. Fulop, L. Kohidai, A short-run new analytical ultracentrifugal micromethod for determining low-density lipoprotein sub-fractions using Schlieren refractometry, Eur. Biophys. J. 29 (2001) 621–627.

[10] J. Lebowitz, M. Teale, P. Schuck, Analytical band centrifugation of proteins and protein complexes, Biochem. Soc. Trans. 26 (1998) 745–749.

[11] J. Lebowitz, M.S. Lewis, P. Schuck, Modern analytical ultracentrifugation in protein science: a tutorial review, Protein Sci. 11 (2002) 2067–2079.

[12] W. Mächtle, in: S.E. Harding, A.J. Rowe, J.C. Horton (Eds.), Analytical Ultracentrifugation in Biochemistry and Polymer Science, The Royal Society of Chemistry, Cambridge, 1992, pp. 147–175.

[13] R. Bruner, J. Vinograd, The evaluation of standard sedimentation coefficients of sodium RNA and sodium DNA from sedimentation velocity data in concentrated NaCl and CsCl solutions, Biochim. Biophys. Acta 108 (1965) 18–29.

[14] C.R. McEwen, Tables for estimating sedimentation through linear concentration gradients of sucrose solution, Anal. Biochem. 20 (1967) 114–149.

[15] R.W. Clark, Calculation of $s_{20,w}$ values using ultracentrifuge sedimentation data from linear sucrose gradients, an improved, simplified method, Biochem. Biophys. Acta 428 (1976) 269–274.

[16] W. Hirst, R.A. Cox, The construction and analysis of sucrose gradients for use with zonal rotors, Biochem. J. 159 (1976) 259–265.

[17] M. Dishon, G.H. Weiss, D.A. Yphantis, Kinetics of sedimentation in a density gradient, Biopolymers 10 (1971) 2095–2111.

[18] O. Lamm, Die Differentialgleichung der Ultrazentrifugierung, Ark. Mat. Astr. Fys., Part B 21 (2) (1929) 1–4.

[19] W.K. Sartory, H.B. Halsall, J.P. Breillatt, Simulation of gradient and band propagation in the centrifuge, Biophys. Chem. 5 (1976) 107–135.

[20] A.P. Minton, Simulation of the time course of macromolecular separations in an ultracentrifuge. I. Formation of a cesium chloride density gradient at 25 °C, Biophys. Chem. 42 (1992) 13–21.

[21] J.S. Philo, An improved function for fitting sedimentation velocity data for low molecular weight solutes, Biophys. J. 72 (1997) 435–444.

[22] J. Behlke, O. Ristau, Molecular mass determination by sedimentation velocity experiments and direct fitting of the concentration profiles, Biophys. J. 72 (1997) 428–434.

[23] W.F. Stafford, Time difference sedimentation velocity analysis of rapidly reversible interacting systems: determination of equilibrium constants by global non-linear curve fitting procedures, Biophys. J. 74 (2) (1998) A301.

[24] P. Schuck, Sedimentation analysis of noninteracting and self-associating solutes using numerical solutions to the Lamm equation, Biophys. J. 75 (1998) 1503–1512.

[25] P. Schuck, C.E. MacPhee, G.J. Howlett, Determination of sedimentation coefficients for small peptides, Biophys. J. 74 (1998) 466–474.

[26] P. Schuck, D.B. Millar, Rapid determination of molar mass in modified Archibald experiments using direct fitting of the Lamm equation, Anal. Biochem. 259 (1998) 48–53.

[27] P. Schuck, B. Demeler, Direct sedimentation analysis of interference optical data in analytical ultracentrifugation, Biophys. J. 76 (1999) 2288–2296.

[28] B. Demeler, J. Behlke, O. Ristau, Determination of molecular parameters from sedimentation velocity experiments: whole boundary fitting using approximate

and numerical solutions of the Lamm equation, Method. Enzymol. 321 (2000) 36–66.
[29] P. Schuck, P. Rossmanith, Determination of the sedimentation coefficient distribution by least-squares boundary modeling, Biopolymers 54 (2000) 328–341.
[30] P. Schuck, Size distribution analysis of macromolecules by sedimentation velocity ultracentrifugation and Lamm equation modeling, Biophys. J. 78 (2000) 1606–1619.
[31] P. Schuck, M.A. Perugini, N.R. Gonzales, G.J. Howlett, D. Schubert, Size-distribution analysis of proteins by analytical ultracentrifugation: strategies and application to model systems, Biophys. J. 82 (2002) 1096–1111.
[32] J. Behlke, O. Ristau, A new approximate whole boundary solution of the Lamm differential equation for the analysis of sedimentation velocity experiments, Biophys. Chem. 95 (2002) 59–68.
[33] P. Schuck, A model for sedimentation in inhomogeneous media. II. Compressibility of aqueous and organic solvents, Biophys. Chem. 108 (2003) 201–214.
[34] H. Fujita, Mathematical Theory of Sedimentation Analysis, Academic Press, New York, 1962.
[35] E.F. Cassassa, H. Eisenberg, Thermodynamic analysis of multicomponent systems, Adv. Protein Chem. 19 (1964) 287–395.
[36] C. Ebel, H. Eisenberg, R. Ghirlando, Probing protein–sugar interactions, Biophys. J. 78 (2000) 385–393.
[37] J.-M. Claverie, H. Dreux, R. Cohen, Sedimentation of generalized systems of interacting particles. I. Solution of systems of complete Lamm equations, Biopolymers 14 (1975) 1685–1700.
[38] C. Tanford, Physical Chemistry of Macromolecules, Wiley, New York, 1961.
[39] J.-M. Claverie, Sedimentation of generalized systems of interacting particles. III. Concentration-dependent sedimentation and extension to other transport methods, Biopolymers 15 (1976) 843–857.
[40] H. Fujita, Foundations of Ultracentrifugal Analysis, Wiley, New York, 1975.
[41] J. Garcia De La Torre, M.L. Huertas, B. Carrasco, Calculation of hydrodynamic properties of globular proteins from their atomic-level structure, Biophys. J. 78 (2000) 719–730.
[42] L. Costenaro, C. Ebel, Thermodynamic relationships between protein-solvent and protein–protein interactions, Acta Crystallogr. D. Biol. Crystallogr. 58 (2002) 1554–1559.
[43] L. Costenaro, G. Zaccai, C. Ebel, Link between protein–solvent and weak protein–protein interactions gives insight into halophilic adaptation, Biochemistry 41 (2002) 13245–13252.
[44] H.K. Schachman, Ultracentrifugation in Biochemistry, Academic Press, New York, 1959.
[45] H. Fujita, J. Am. Chem. Soc. 63 (1956) 1092.
[46] J.P. Johnston, A.G. Ogston, A boundary anomaly found in the ultracentrifugal sedimentation of mixtures, Trans. Faraday Soc. 42 (1946) 789–799.
[47] J.J. Correia, M.L. Johnson, G.H. Weiss, D.A. Yphantis, Numerical study of the Johnston–Ogston effect in two-component systems, Biophys. Chem. 5 (1976) 255–264.
[48] J. Vinograd, J.E. Hearst, Equilibrium sedimentation of macromolecules and viruses in a density gradient, Fort. Chem. Org. Nat. 20 (1962) 372–422.
[49] D.J. Cox, R.S. Dale, in: C. Frieden, L.W. Nichol (Eds.), Protein–protein Interactions, Wiley, New York, 1981.
[50] M.J. Rosovitz, P. Schuck, M. Varughese, et al., Alanine scanning mutations in anthrax toxin protective antigen domain 4 reveal residues important for binding to the cellular receptor and to a neutralizing monoclonal antibody', J. Biol. Chem. 278 (2003) 30936–30944.
[51] R.C. Weast, Handbook of Chemistry and Physics, CRC Press, Cleveland, OH, 1972.